Artificial Organs

A Computational Model of Heat Loss and Water Condensation on the Gas-Side of Blood Oxygenators

Ricardo Gómez Bardón, Gabriele Dubini, and Giancarlo Pennati

Department of Chemistry, Materials and Chemical Engineering "Giulio Natta", Politecnico di Milano, Milan, Italy

Abstract: Clinical observation of condensation at the gas flow exit of blood oxygenators is a recurrent event during cardiopulmonary bypass. These devices consist of a bundle of hollow fibers made of a microporous membrane that allows the exchange of O_2 and CO_2. The fibers carry a gas mixture inside (intraluminal flow), while blood flows externally around them (extraluminal flow). Although different studies described this effect in the past, the specific role of the different sections of the device requires further analysis, and the total condensation rate remains unquantified. In this study, a closer look is taken at the transition of gas between the oxygenation bundle and the external room air. A method is proposed to estimate the total condensate output, combining computational fluid dynamics (CFD) of thermal distribution and a simplified 1D model of water vapor saturation of gas. The influence of a number of different parameters is analyzed, regarding material properties, environmental conditions, and clinical use. Results show that condensation rate could vary in a 30-fold range within reasonably small variations of the different variables considered. **Key Words:** Blood oxygenator—Condensation—Hollow fiber membrane—Heat exchange—Computational fluid dynamics.

Cardiopulmonary bypass (CPB) is performed during open-heart surgeries when the patient's heart and lungs need to stop functioning, as well as during extracorporeal life support for patients with severe respiratory and/or heart diseases. The blood is collected from the venous circulation and diverted to an extracorporeal circuit, where it is oxygenized and pressurized before being redirected to the arterial systemic circulation. A blood pump replaces the heart function, while a blood oxygenator provides the gaseous exchange.

Blood oxygenators have experienced several changes in the past 50 years (1), and currently, the oxygenating module consists of a bundle of polymeric hollow fibers that carry the gaseous mixture (usually, nitrogen, and oxygen), with the blood flowing externally around them. The microporous semipermeable membrane of the fibers allows oxygen (O_2) and carbon dioxide (CO_2) exchange between the extraluminal (blood) and intraluminal (gas) flows.

Due to the microporous nature of the membrane, blood plasma can evaporate at the liquid-membrane interface and diffuse as water vapor across the pores into the intraluminal gas phase. Despite being the supplied gaseous mixture dry, due to the large water vapor mass transfer coefficients of the microporous membranes, the gas is expected to become highly saturated within a short fiber length (2). However, a theoretical investigation of the thermal behavior of gas flowing through an oxygenator (3) pointed out that water vapor cannot condense within the oxygenating bundle. Indeed, the surrounding blood warms up the gas when it enters the fibers, and gas temperature equals that of blood almost instantly.

Anyhow, clinical observation of condensate at the gas flow exit is still a common event. It is normally associated with the sudden cooling of the gas flow in the proximity of the outlet cover (after

doi: 10.1111/aor.13277

Received December 2017; revised March 2018; accepted April 2018.

Address correspondence and reprint requests to Ricardo Gomez Bardon, Dipartimento di Chimica Materiali e Ingegneria Chimica Giulio Natta Politecnico di Milano, Piazza Leonardo da Vinci, 32 Milano 20131, Italy. E-mail: ricardo.gomez@polimi.it

exiting the fiber bundle), where the warming effect of blood is no longer present (3). The condensate could progressively obstruct a certain number of fibers, reducing the effective membrane surface area for gaseous exchange. Therefore, a number of studies investigated possible strategies for preventing or limiting water condensation: by warming the gas at the inflow (4) or outflow section (5), creating a warm environment around the whole oxygenator (6), or blowing off the condensate from the clogged fibers by gas flushing (7).

The current study focuses on water condensation rate when the gas flows through the outlet region of an oxygenator, where the gas temperature decreases. Namely, two different regions are identified outside the oxygenating bundle: (i) the gas outlet cover and (ii) the transition region between the oxygenating bundle and the oxygenator case, where a polymeric resin is used for holding the fiber bundle together and isolating the blood volume from the rest of the device. Within a blood oxygenator, two different transition regions exist, placed at the beginning and at the end of the oxygenating bundle respectively. In this article, we will indicate them as "upstream" and "downstream" transition, with reference to the gas flow direction. In particular, the downstream transition region is expected to generate greater thermal losses, eventually leading to gas condensation within the hollow fibers.

The goal of this article is to describe in detail the temperature map of the gas along the outlet portion of a blood oxygenator by means of 3D computational fluid dynamics (CFD), and to estimate water condensation rates in the downstream transition coupling the temperature results to a simplified 1D model of water vapor transport and condensation (2). The influence of different parameters is evaluated, regarding the oxygenator design, material properties of the transition, environmental conditions, and clinical use.

MATERIALS AND METHODS

The water vapor within the gas mixture flowing through the fibers of an oxygenator may be quantified by the relative humidity RH:

$$\mathrm{RH} = {}^{\rho_{\mathrm{fiber}}}\!/_{\rho_{\mathrm{sat}}(T)}$$

where ρ_{fiber} is the mass concentration (kg/m) of water vapor inside the fiber and $\rho_{\mathrm{sat}}(T)$ is[3] the mass concentration corresponding to a fully saturated gas, which depends on the gas temperature T (see Gas-side water saturation inside the oxygenating bundle section for details).

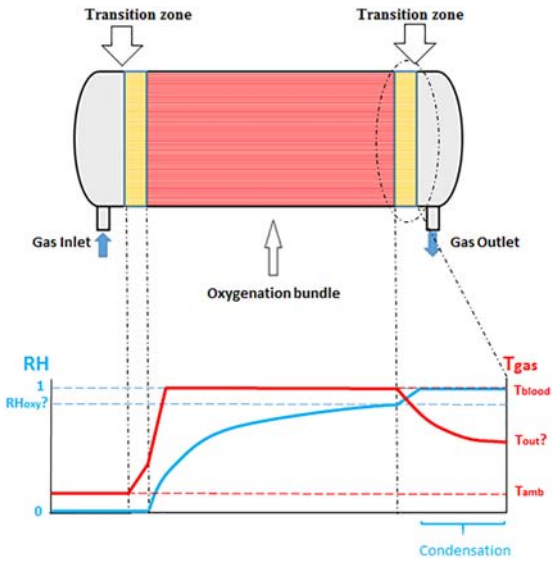

FIG. 1. Blood oxygenator outline, with estimation of the temperature and saturation distribution along its different sections. [Color figure can be viewed at wileyonlinelibrary.com]

In this study, we disregard metastatic states, and therefore $\mathrm{RH} \leq 1$, that is, $\rho_{\mathrm{fiber}} \leq \rho_{\mathrm{sat}}(T)$. Hence, water condensation will occur whenever the water vapor content inside the fibers tries to exceed the value of $\rho_{\mathrm{sat}}(T)$. As $\rho_{\mathrm{sat}}(T)$ decreases when T decreases, the condensation rate within the fibers depends both on water vapor content and gas temperature. Consequently, two different processes are involved: the water vapor transfer from blood to gas within the oxygenating bundle, and the heat transfer from blood to gas as well as from gas toward the surrounding environment.

Under some reasonable assumptions, the two transfer phenomena may be associated to different sections of the device: increase in RH across the oxygenating bundle and heat losses across the downstream transition. Within the oxygenating bundle, water vapor enters the gas side due to the microporous nature of the fiber membrane, increasing its RH toward full saturation (2). At the same time, the gas flow starts to warm up in the upstream transition and reaches the blood temperature (T_{b}) after a trivial length of the oxygenating bundle (3) (Fig. 1), due to the negligible thermal inertia of gas compared to the surrounding blood. Along the bundle, the fibers are surrounded by warm blood, with a thermal effect that outweighs the influence of cold air from the environment surrounding the device (3). Consequently, the gas inside the fibers is hardly cooled down within the

oxygenating bundle and condensation cannot occur in this region, despite RH could be virtually equal to one. On the contrary, condensation is expected to occur when the gas enters the downstream transition, as fibers are no longer surrounded by blood and the gas temperature decreases, reducing $\rho_{sat}(T)$.

Overall, condensation rate within the fibers will depend both on the ρ_{fiber} at the inlet of the downstream transition (i.e., at the end of the oxygenating bundle) and on the temperature at the outlet of the downstream transition. Both factors, in turn, depend on the design parameters of the device, environmental conditions and mode of use.

To compute the total condensation rate associated with all these variables, the following methodology is adopted:

1. A simplified 1D model is used to calculate the water saturation of gas within the fibers along the oxygenating bundle;
2. A CFD 3D parametric model is developed to evaluate the gas temperature field in the downstream transition and outlet cover;
3. Results from the two previous sections are combined to calculate the condensation rate inside the downstream transition.

Each of these steps is described in detail in the following sections.

Gas-side water saturation inside the oxygenating bundle

Our goal is to derive an analytic equation describing the RH change along the oxygenating bundle as a function of the axial position. The following assumptions are considered:

- the gaseous mixture inside the fibers and within the membrane pores behaves like an ideal gas;
- the system is at steady state and thermal equilibrium;
- both phases (gas and blood) are at the same temperature throughout the entire oxygenating bundle, and therefore no significant temperature gradient is observed in this region ($T = T_b$);
- the pore size is small enough to prevent liquid from entering the gas-side;
- within the membrane pores, the water vapor partial pressure in the gas mixture equals the water vapor tension of the liquid phase;
- all fibers have an identical gas volumetric flow rate q_{fiber};
- q_{fiber} is constant along a single fiber, disregarding slight variations due to gas and water vapor exchange across the membrane.

Under these simplifications, the mass balance of water vapor in an infinitesimal length dz of a single fiber within the oxygenating bundle is:

$$q_{fiber} d(\rho_{fiber}(z)) = K_m \pi D (\rho_{sat}(T_b) - \rho_{fiber}(z)) dz$$

where:

- z is the axial position along the oxygenating bundle (m);
- $\rho_{fiber}(z)$ is the mass concentration of water vapor in the gas fiber at z (kg/m^3);
- $\rho_{sat}(T_b)$ is the mass concentration of saturated water vapor (kg/m^3) at the membrane-blood interface at blood temperature;
- D is the fiber outer diameter (m);
- K_m is the water vapor transfer coefficient (m/s) across the microporous membrane.

Integration of the above expression yields:

$$\rho_{fibre}(z) = \rho_{sat}(T_b)\left(1 - e^{-\frac{K_m \pi D}{\rho_{fibre}} z}\right)$$

In terms of RH, considering the gas temperature T equal to T_b, we have:

$$RH(z) = \frac{\rho_{fiber}(z)}{\rho_{sat}(T_b)} = \left(1 - e^{-\frac{K_m \pi D}{q_{fiber}} z}\right)$$

and, for $z = L_{oxy}$ (being L_{oxy} the total length of the oxygenating bundle):

$$RH_{OXY} = \left(1 - e^{-\frac{K_m \pi D}{q_{fiber}} L_{oxy}}\right)$$

This represents how saturated the gas flow arrives at the downstream transition, just after the end of the oxygenating bundle.

The above relation can be expressed in terms of the total oxygenating membrane area of the fiber bundle. Considering that under our assumptions all fibers carry the same flow:

$$\left.\begin{aligned} q_{fiber} &= Q_g / N_{fibers} \\ N_{fibers} &= A_{OXY} / \pi \cdot D \cdot L_{oxy} \end{aligned}\right\} \; RH_{OXY} = \left(1 - e^{-\frac{K_m \cdot A_{OXY}}{Q_g}}\right)$$

where:

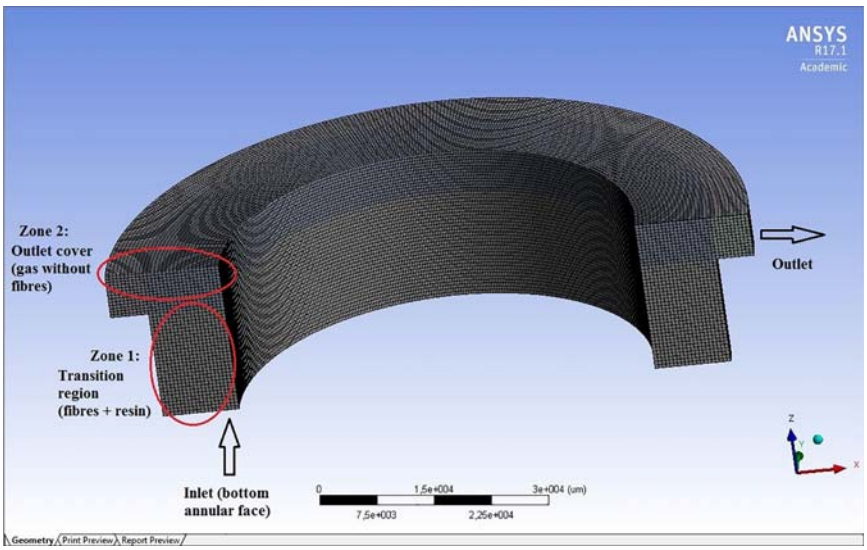

FIG. 2. Three-dimensional model for CFD analysis. [Color figure can be viewed at wileyonlinelibrary.com]

- Q_g (m^3/s) is the total gas flow rate across the entire device;
- N_{fibers} is the total number of fibers in the oxygenating bundle;
- A_{OXY} (m^2) is the total membrane area in the bundle.

Similarly to RH(z), we can describe the variation of water vapor saturation along the fiber bundle in terms of the membrane area, RH(A_M), being A_M the portion of membrane area up to a certain axial location z.

$$RH(A_M) = \left(1 - e^{-\frac{K_m \cdot A_M}{Q_g}}\right)$$

Looking at the expression above, we realize that the saturation level of the gas only depends on the membrane water vapor permeability (K_m), the membrane area (A_M), and the total gas flow (Q_g) through the device, independently of the oxygenating bundle microstructure (fiber diameter and arrangement) or geometrical dimensions (bundle cross-sectional area and length).

Temperature distribution along the transition region

A 3D model representing a typical outlet section of a blood oxygenator was designed using ANSYS 17.1 Design Modeler (ANSYS Inc, Canonsburg, PA, USA). The model consists of a hollow cylinder (Fig. 2), as this is a common geometry for commercial oxygenating bundles. Two different regions can be distinguished in the model, that is, the downstream transition (fibers carrying gas surrounded by resin) and the gas outlet cover (gas flowing freely without fibers).

Gas enters the model through the bottom annular face of the downstream transition (zone 1), which would be connected to the end of the oxygenating bundle and exits through an opening in the gas outlet cover (zone 2). For the sake of simplicity in meshing, the outlet window is assumed rectangular and an outlet pipe is not considered.

The downstream transition is represented with the Porous Media model, which adds a momentum loss term to the Navier–Stokes equations (8). The main parameters characterizing the porous media are the viscous resistance, the thermal conductivity and the porosity. The first one determines the fluid dynamic behavior, while the other two influence the thermal behavior following the equation (8)

$$k_{eff} = \varnothing \cdot k_g + (1 - \varnothing) \cdot k_{trans}$$

where k_{eff} is the averaged thermal conductivity in the porous media domain, ø is the porosity, and k_{trans} and k_g are the thermal conductivities of resin and gas, respectively.

The adopted viscous resistances (inverse of the porous media permeability) are 1.2×10^9 m^{-2} and 1.2×10^{12} m^{-2} for axial and radial directions, respectively. The axial value is calculated analytically for an oxygenating bundle of longitudinal fibers with an internal diameter of 280 μm, and density of 550 fibers/cm^2. Despite different fiber microstructure arrangements could modify this value, the viscous resistance only influences the pressure drop across the downstream transition, without significant effects on the thermal behavior.

Moreover, considering the temperature and pressure drops involved, we can assume the gas fluid dynamic behavior to be uncoupled with the thermal field. The radial viscous resistance is set 1000 times higher so that the flow is forced to move axially (as the gas is confined inside the fibers). Values for thermal conductivity and porosity are described in Considered values section.

The fluid model implemented in Fluent is pure O_2 ($\rho = 1.3$ kg/m^3; $\mu = 1.92 \cdot 10^{-5}$ Pa s; $k_g = 0.0246$ W/m K), considered as an ideal gas. The flow was modelled as incompressible (Mach number in the order of 10^{-4}, and pressure drops across the model in the range of 2 mm Hg) and laminar. The Reynolds number is in the range of 2 inside the fiber lumen and 200 in the outlet cover. The resin of the transition is characterized as $\rho = 1200$ kg/m^3; $k = k_{trans}$ (see Considered values section for details).

The temperature at the inlet of the model and on the internal walls (i.e., toward the oxygenator core) is set to 37°C (blood temperature), while the external walls (in contact with room environment, at 20°C) have heat convection boundary condition. The plastic case of the oxygenator is not meshed but is included in the thermal wall boundary conditions of the model, with a thickness t (see Considered values section for specific values).

The geometries are meshed in ANSYS 17.1 Workbench (ANSYS Inc). For the sake of simplicity, only half of the geometry is meshed, taking advantage of the symmetry plane, as can be seen in Fig. 2. The number of mesh elements is 1.4×10^6, all of them hexahedral with an average quality of 0.96. A mesh independence study was performed by successively refining an initial mesh by an overall factor around 1.5, focusing on the external diameter of the transition region (ø, corresponding to the highest temperature gradients). When 1.4×10^6 elements were reached, the temperature field in the successive refining differed by less than 0.01°C. Similarly, a convergence study was carried out changing the convergence criteria from 10^{-4} to 10^{-6}.

A sensitivity analysis is performed for some parameters affecting the thermal distribution in the transition region. These are the thermal conductivity of the resin (k_{trans}), the convection coefficient of the surrounding environment (h), the porosity (ø, corresponding to different fiber densities in the oxygenating bundle), the thickness of the plastic case of the device, and the total gas flow going through the oxygenator (Q_g).

The temperature distribution along the axial and radial directions inside the downstream transition is analyzed and compared by varying one parameter at a time, so that the influence of each one can be isolated. The simulations do not consider any change of phase, and so disregarded the latent heat released by water when condensing. This hypothesis is verified in Results section, once the total amount of condensation is calculated.

Condensation rate inside the downstream transition

Once the gas reaches the inlet of the downstream transition (with $T = T_b$), it cools down following the temperature distribution obtained in the CFD analysis. This temperature drop reduces ρ_{sat}, increasing RH and leading to condensation.

To compute the ρ_{sat} value as a function of temperature, we consider the relation for one of the components in a perfect gas mixture:

$$\rho_{sat}(T) = \frac{p^*(T)}{R_{wv} T}$$

and the Antoine equation (9)

$$\mathrm{Log}(p^*) = 5.94641 - \frac{1730.63}{T - 40.074}$$

with p^* in Pa, ρ_{sat} in kg/m^3, T in K, and the gas constant $R_{wv} = 8.314/M_{wv}$ (J/kg K), where M_{wv} is the molecular weight of water vapor equal to 18 kg/kmol.

Inside a single fiber, the condensation rate is equal to the difference between the water vapor dissolved in gas at the inlet (i.e., end of the oxygenating bundle) and the outlet (i.e., the fiber tip) of the downstream transition, multiplied by the gas flow inside the fiber. Within our simplified model, we consider the amount of water dissolved at the fiber tip equal to the saturation density of gas at the fiber tip temperature.

Therefore, we have

$$Q_{\mathrm{cond\ fiber}}\left[\frac{\mathrm{kg}}{\mathrm{s}}\right] = q_{\mathrm{fiber}}\left[\frac{\mathrm{m}^3}{\mathrm{s}}\right] \cdot -\Delta\rho_{\mathrm{water}}\left[\frac{\mathrm{kg}}{\mathrm{m}^3}\right] = q_{\mathrm{fiber}} \cdot \left(\mathrm{RH}_{\mathrm{OXY}} \cdot \rho_{\mathrm{sat}}(T_b) - \rho_{\mathrm{sat}}\left(T_{\mathrm{fiber\ tip}}\right)\right)$$

The total condensate in the downstream transition can be computed by integrating the above expression along the surface corresponding to the fiber tips. This has to be applied only to the fibers with $\mathrm{RH}_{\mathrm{OXY}} \cdot \rho_{\mathrm{sat}}(T_b) \geq \rho_{\mathrm{sat}}\left(T_{\mathrm{fiber\ tip}}\right)$, as the other fibers do not reach RH = 1 within the transition -

therefore condensate does not form - and shall not be included in the integral. Using the same variables from the previous sections, and recalling that the gas flow is homogeneously distributed across all fibers, we have:

$$Q_{\text{cond}} = \int_{A_{\text{tips}*}} q_{\text{fiber}} \cdot \left(\text{RH}_{\text{OXY}} \cdot \rho_{\text{sat}}(T_{\text{b}}) - \rho_{\text{sat}}\left(T_{\text{fiber tip}}\right)\right)$$

$$dA = Q_{\text{g}} \frac{A_{\text{tips}*}}{A_{\text{tips}}} \cdot \left[\text{RH}_{\text{oxy}} * \rho_{\text{sat}}(T_{\text{b}}) - \overline{\rho_{\text{sat}}(T)}\big|_{A_{\text{tips}*}}\right]$$

where $A_{\text{tips}*}$ represents the area of fiber tips with condensation, while A_{tips} corresponds to the total area of the fiber tips surface. The last term represents the average value of the saturation density at the $A_{\text{tips}*}$.

As previously mentioned, the latent heat released by water vapor when condensing is taken as negligible, what could in principle alter the temperature field along the fibers obtained by CFD.

Once we have calculated the condensation rate, the temperature variation associated with the released latent heat (ΔT_{cond}) may be calculated as follows:

$$Q'_{\text{lat fiber}} = \dot{\text{m}}_{\text{gas fiber}} \cdot \text{Cp}_{\text{gas}} \cdot \Delta T_{\text{cond}}$$

where $\text{Cp}_{\text{gas}} = 1$ (kJ/kg K) is the heat capacity of the gas, $\dot{m}_{\text{gas fiber}}$ (kg/s) is the mass flow rate in a single fiber ($\dot{m}_{\text{gas fiber}} = q_{\text{g}} \cdot \rho_{\text{gas}}$), and $Q'_{\text{lat fiber}}$ (W) the latent heat released within a single fiber due to condensation

$$Q'_{\text{lat fiber}} = \dot{\text{m}}_{\text{cond fiber}} \cdot h_{\text{w,lat}}$$

with $h_{\text{w, lat}} = 2.26$ kJ/kg (latent heat of water at 100°C). Conversely, we have

$$\dot{\text{m}}_{\text{cond fiber}} = q_{\text{fiber}} \cdot \Delta\rho_{\text{fiber}} = q_{\text{fiber}} \cdot \left(\rho_{\text{sat}}(T_{\text{b}}) - \rho_{\text{sat}}\left(T_{\text{tip}}\right)\right)$$

and combining all the above expressions we obtain:

$$\Delta T_{\text{cond}} = \frac{h_{\text{w,lat}} \cdot \left(\rho_{\text{sat}}(T_{\text{b}}) - \rho_{\text{sat}}\left(T_{\text{tip}}\right)\right)}{\rho_{\text{air}} \cdot \text{Cp}_{\text{gas}}}$$

Considered values

In this study, we focus on adult sizes of blood oxygenators used in cardiopulmonary bypass, in surgery under normothermia (i.e., blood at 37°C). Considering the wide range of different blood oxygenator designs available in the market, the effects of both radial and axial extension of the downstream transition are analyzed. A standard geometry (Fig. 2) is identified with a cross-sectional area of 2000 mm^2 (internal and external diameters of 55 and 75 mm, respectively), and a transition length of 15 mm, making a total resin volume of approximately 30 cm^3, in line with commercial models for adult use. Moreover, two variants are considered. A first variant has a cross-sectional area of 4000 mm^2 (internal and external diameters of 70 and 100 mm, respectively), while the second variant has a transition length of 25 mm. Different diameters represent a range of patient sizes, whereas the transition length is more a technological consideration, balancing the structural integrity of the device and total resin volume. The main geometric dimensions of the three geometries are summarized in Table 1.

TABLE 1. *Main geometric dimension*s

Geometry	Standard (mm)	Wider radius (mm)	Longer transition (mm)
Internal diameter, D_{int}	55	70	55
External diameter, D_{ext}	75	100	75
Transition length, L_{trans}	15	15	25
Gas outlet cover height		6	

Normal gas flows used during open-heart surgeries in adults range from 2 to 7 Lpm, while the total membrane surface area is around 1.5 and 2 m^2 in a typical adult size of an oxygenator (10). As for the significant values of the membrane water vapor transfer coefficient K_{m}, there is relatively scarce data available in the literature referring to microporous hollow fibers used in blood oxygenators. A typical range would be $K_{\text{m}} = 1 \times 10^{-3} \div 1 \times 10^{-4}$ m/s (11), and considering the porous nature of the fiber membrane, K_{m} is likely to take values in the high-end of this range, if not higher.

With reference to the parameters analyzed in the CFD simulations, the thermal conductivity k_{trans}, is quite difficult to characterize and requires some special considerations. First of all, it should be noticed that the porous media model only allows a single value for the thermal conductivity (8), while in reality the medium in the downstream transition is composed by the polymeric resin and the fiber microporous membrane (HDPE). Moreover, different manufacturers provide a relatively wide range of values for thermal conductivity of polymeric resins, subject to natural variances due to the manufacturing process. Based on the available

TABLE 2. *Sensitivity parameters and values considered*

Parameter	Group	Reference value	Sensitivity values
Total gas flow: Q_g (Lpm)	Operation conditions	5	2; 7
Resin conductivity: k_{trans} (W/m K)	Device design	0.2	0.02; 1
Room convection: h (W/m^2 K)	Operation conditions	5	0.5; 10
Porous medium porosity: $\varnothing$	Device design	0.4	0.3; 0.5
Plastic case thickness: t (mm)	Device design	2.5	5

literature (12), 0.2 W/m K is taken as a standard value, and 0.02 and 1 as sensitivity values. Although the lower value would typically correspond to an isolating foam, it makes sense to include it here to account for the effect of the microporous membrane. Previous studies of thermal properties of resin and HDPE composite materials reported conductivity values in the same range (13).

As for the rest of the parameters, the standard value for the convective heat transfer coefficient h is taken as 5 W/m^2 K, corresponding to a natural convection around a cylinder (14), while the sensitivity values are 0.5 and 10, representing more isolated or ventilated environments, respectively (being the latter situation more likely to occur in an operating theatre). The considered porosities are $\varnothing$ = 0.3, 0.4, and 0.5, being 0.4 a typical value for a commercial model (values out of this range would not be representative of an oxygenating bundle). The plastic case thicknesses, t, considered are 2.5 and 5 mm. Finally, the standard Q_g is 5 Lpm, also considering 2 and 7, representing different clinical requirements during a CBP intervention. The values of these properties are summarized in Table 2.

RESULTS

The expression for RH(A_M) is plotted for the different values of interest. As it can be seen in Fig. 3, with the exception of high flows in the low range of K_m values, gas becomes fully saturated inside the oxygenating bundle, and so it reaches the downstream transition with a water content corresponding to $RH_{oxy} = 1$. For the cases of 5 and 7 Lpm with $K_m = 1 \times 10^{-4}$ m/s, saturation levels reach around 80% for the range of commercial adult sizes.

As for the CFD temperature distributions, the standard geometry from Table 1 is first simulated with all reference values for all parameters listed in Table 2, yielding the temperature map along the downstream transition shown in Fig. 4A. It should be noted that the room temperature, equal to 20°C, is applied in the CFD model to the external face of the plastic case (not shown), while Fig. 4A shows the air temperature inside the outlet cover. As expected, gas flows axially through the fiber bundle and then circumferentially through the cover toward the outlet window, accelerating as it comes closer to the exit.

The temperature distribution shows a dependency on the circumferential direction (Fig. 4B),

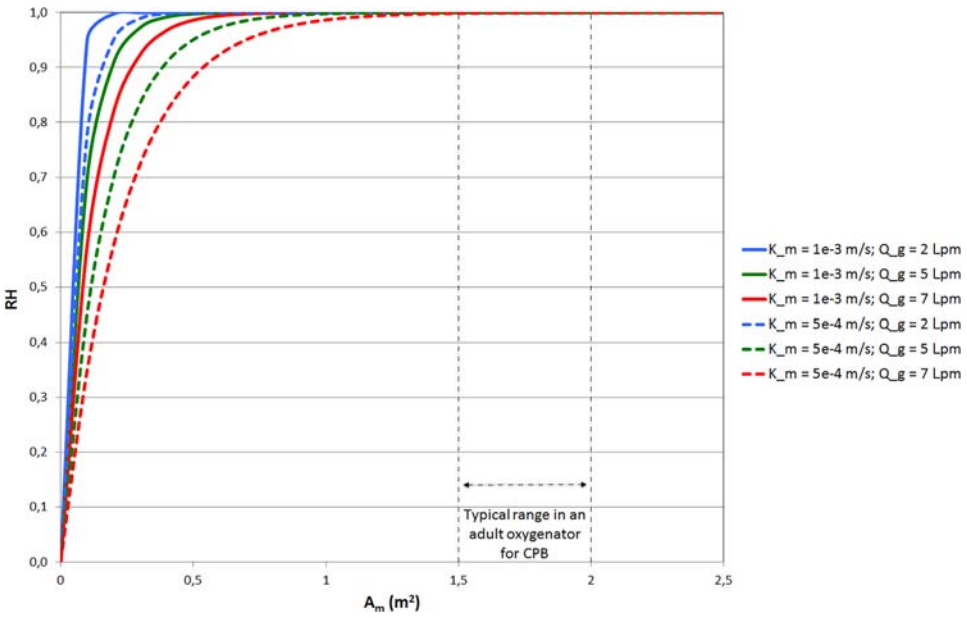

FIG. 3. Water saturation inside the oxygenating bundle. [Color figure can be viewed at wileyonlinelibrary. com]

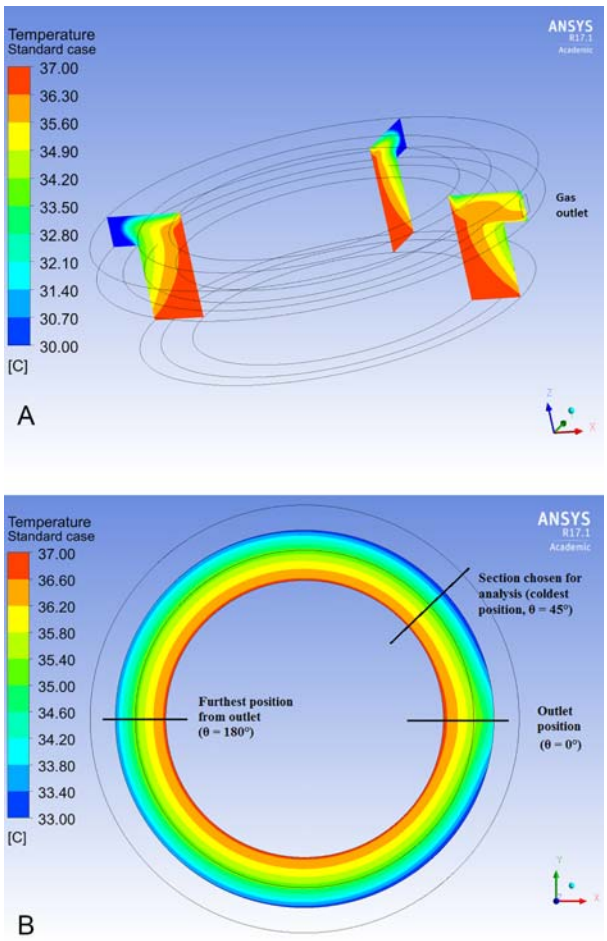

FIG. 4. (A) Temperature profile along the downstream transition in the standard case. (B) Temperature map at the end of the transition (corresponding to the fiber tips). [Color figure can be viewed at wileyonlinelibrary.com]

due to the concentration of gas toward the outlet window. Hence, in the subsequent analyses, we focus only on the circumferential plane with the maximum temperature drop (5°C for the standard case), located at $\theta = 45°$. Moreover, the temperature distribution is reported in terms of cooling from the oxygenating bundle, that is, $\Delta T = T\ (°C) - 37$.

The different geometries are accounted by normalizing both the axial and radial dimensions in the following way:

1. Normalized axial position, $z^* = z/L_{trans}$, being $z^* = 0$ the start of the transition region and $z^* = 1$ the end, along the gas flow direction.
2. Normalized radial position, $r^* = (r - D_{int}/2)/R_{trans}$, with $R_{trans} = (D_{ext} - D_{int})/2$, being $r^* = 0$ the internal wall, in contact with the oxygenator core, and $r^* = 1$ at the external wall.

The first parameter to be analyzed is k_{trans}; Fig. 5A shows its influence in the axial direction, along a fiber next to the external wall ($r^* = 0.98$, accounting for the fiber thickness). The temperature cools down in a nonlinear manner, with lower values of k_{trans} leading to a higher ΔT. Moreover, Fig. 5B shows the ΔT along the fiber tips ($z^* = 1$), showing that the curves for different k_{trans} intersect each other and change their relative position. In a similar manner, the influence of h and Q are studied, obtaining analogous curves to Fig. 5 which are not reported for conciseness.

Figure 6A collects the values of the maximum ΔT ($z^* = 1$, $r^* = 0.98$, $\theta = 45°$) for each case. Both $\varnothing$ and t have negligible effects (under 2% for the maximum ΔT, and around 1% for the condensation rate), and therefore, we only report the results

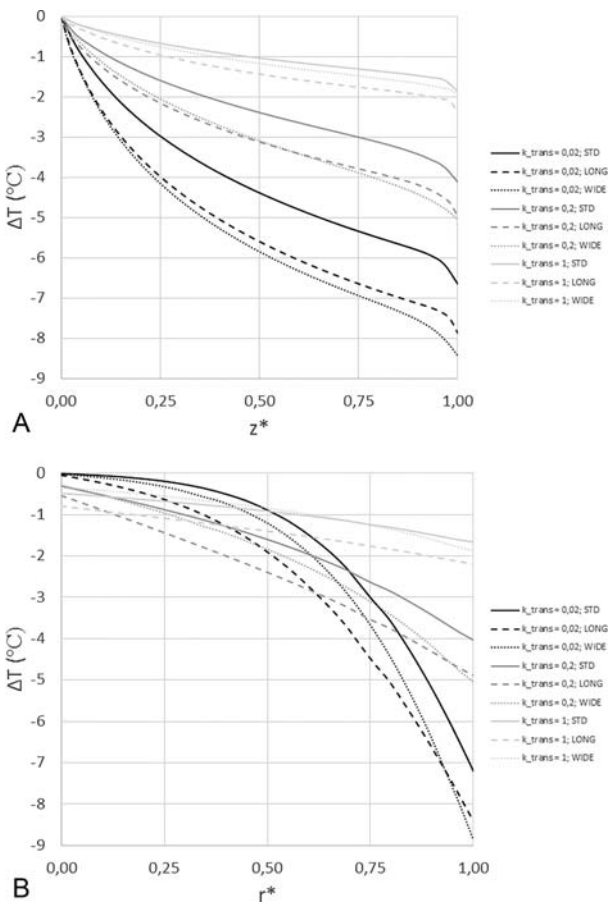

FIG. 5. (A) Temperature drop along the external fiber ($r^* = 0.98$) varying the resin thermal conductivity, k_{trans} (W/m K). "STD" stands for Standard Geometry, "Long" for Longer Transition, and "Wide" for Wider Radius. (B) Temperature drop along the radial direction at the fibers' tip ($z^* = 1$), varying the resin thermal conductivity, k_{trans} (W/m K). "STD" stands for Standard Geometry, "Long" for Longer Transition, and "Wide" for Wider Radius.

corresponding to their standard values (i.e., 0.4 porosity and 2.5 mm thickness). Among all the different cases, the maximum ΔT ranges from 1 to 8°C. It should be noted that, while the standard geometry (with less resin volume) shows lower temperature drop, the relative position of the three geometries varies for each different case studied (varying as well for the condensation rates, as shown in Fig. 7). This indicates the coupled effect of geometry and the rest of the variables.

To calculate total condensation rates, two cases of water vapor saturation are considered, $RH_{oxy} = 0.8$ and $RH_{oxy} = 1$. The former is much less likely to occur in a real blood oxygenator (as discussed below), but is considered here for completeness. Combining these saturation levels with temperature distributions along the downstream transition, total condensation rates are calculated as described in Condensation Rate Inside the Downstream Transition section.

For the most likely case of full saturation ($RH_{oxy} = 1$), Fig. 6B shows the condensation in the coldest fiber, where the effect of Q_g can be noticed by comparison with Fig. 6A. Figure 7 collects the values for the different cases in an analogous

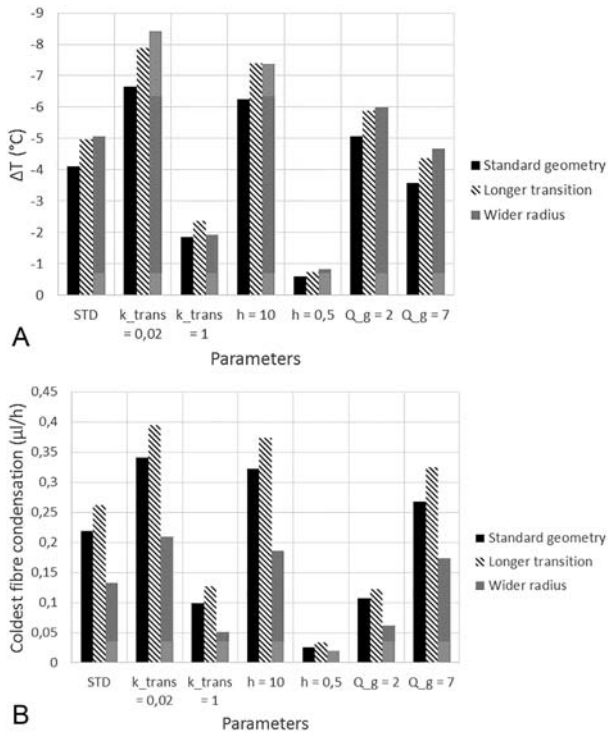

FIG. 6. (A) Estimation of the maximum ΔT generated in the downstream transition, for all the cases considered (k_{trans} in W/m K, h in W/m^2 K, Q_g in Lpm).(B) Estimation of the condensation rate in the coldest fiber, for all the cases considered (k_{trans} in W/m K, h in W/m^2 K, Q_g in Lpm).

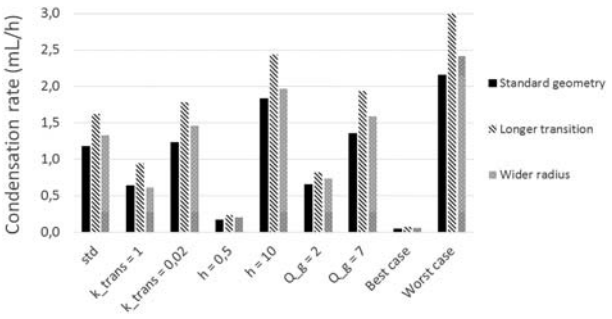

FIG. 7. Estimation of the condensation rate in the entire downstream transition, for RHoxy = 1 (k_{trans} in W/m K, h in W/m^2 K, Q_g in Lpm).

manner, for the entire device. Moreover, the different parameter values are combined in all possible ways to obtain the best- and worst-case scenarios (i.e., lowest and highest condensation output). Interestingly, due to the coupled effect of the parameters, the combinations that lead to best/worst cases in terms of condensation are not the same as for ΔT. Table 3 collects the values for each case. The rainout generated within the entire transition region ranges from 0.1 to 3 mL/h.

For the unlikely case of partial saturation ($RH_{oxy} = 0.8$), water vapor condensates at $\Delta T \geq 5$°C, as follows from Antoine equation. From Fig. 6, we see that only three cases satisfy this, noting that this is the *maximum* ΔT in the whole model, corresponding to the temperature drop in a small section of the fiber tips. Calculations for these three cases give condensation rates of 0.01 mL/h, and zero in the rest (where condensation does not initiate anywhere, because of an insufficient temperature drop).

Finally, the temperature distribution is used to check the validity of the hypothesis of negligible effects of the latent heat release. A worst-case situation of $\Delta T = 13$°C is considered, based on the CFD results, yielding

$$\rho_{sat}(@26^\circ C) = 0.022 \frac{kg}{m^3} \rightarrow \text{Max}\,\Delta T_{cond} = 0.037^\circ C$$

which clearly justifies our assumption.

DISCUSSION AND CONCLUSIONS

The present study identifies causes of water vapor condensation in blood oxygenators during their use and provides a methodology to quantify this rate in relation to different key parameters. The variables analyzed are related both to the device design (k_{trans}, t, ϕ) and clinical use (h, Q),

TABLE 3. *Corresponding values for best- and worst-case scenarios, regarding maximum ΔT and maximum condensation*

Parameter	Worst case max ΔT	Worst case max condense	Best case min ΔT	Best case min condense
Gas flow: Q_g (Lpm)	2	7	7	2
Resin conductivity: k_{trans} (W/m K)	0.02	0.2	1	1
Room convection: h (W/m^2 K)	10	10	0.5	0.5
Porous medium porosity: ∅	Irrelevant			
Plastic case thickness: t (mm)	Irrelevant			
Geometry	Wider radius	Longer transition	Standard	Standard
Total condensation rate (mL/h)	1.46	3	0.17	0.1
Max ΔT (°C)	13	7	0.2	0.5

having different effects on gas temperature drop and condensation rate.

As described above, the saturation level inside the fiber bundle greatly depends on the mass transfer coefficient for water vapor of the microporous membrane (K_m), which is particularly difficult to estimate and is poorly documented in the literature for the particular application of blood oxygenators. For most cases, our simplified model predicts that gas inside the oxygenation bundle quickly becomes heated and humidified by blood, arriving at the downstream transition fully saturated ($RH_{oxy} = 1$) at 37°C, in agreement with previous studies (2,3). Due to thermal losses in this region, the gas cools down becoming supersaturated and initiating condensation. For low values of K_m (combined with high values of Q_g), our model predicts gas saturation levels in the order of 0.8 when arriving at the downstream transition, leading to negligible condensation rates. Such low-range values of K_m would be unlikely in a blood oxygenator, as it would lead to a poor oxygenating performance (being the mass transfer coefficient for water vapor similar to that of oxygen). We compare here the two situations ($RH_{oxy} = 1$ and $RH_{oxy} = 0.8$) to stress the fact that a more accurate characterization of this parameter would contribute to a better design of the device. Again, we point out that results of full saturation are in agreement with previous studies (2,3).

Results show a significant temperature drop of gas inside the fibers in the transition region: up to 9°C within a relatively conservative range of k, h, and Q parameters. This could lead to condensate outputs spanning a 30-fold range, from 0.1 to 3 mL/h, considering the downstream transition region of our standard geometry, with a total intraluminal volume of 10 mL.

As can be seen in Fig. 5A,B, higher conductivities help to homogenize the temperature field along the transition region. Therefore, more conductive materials would reduce the gas temperature drop, minimizing condensation inside the fiber lumen. Conversely, an excessive shortening of the transition length would not be recommended, as other variables like bundle structural integrity or isolation of the blood and gas phases should be also considered. While the difference in the maximum ΔT is much higher for k_{trans} than for Q within the considered range of values (Fig. 6), from Fig. 7 we observe that both k_{trans} and Q have a comparable effect toward condensation. This is mainly due to the thermal distribution in the radial direction (Fig. 5B). Even though the maximum temperature drop increases for lower k_{trans}, the inner fibers are actually warmer, and so the overall effect on condensation is compensated. Moreover, it should be noted that Q has an inverse effect on ΔT and condensation rate (higher values reduce ΔT but increase condensate), due to the fact that condensation depends on both the temperature and the amount of water carried by the gas. This effect is also shown in Fig. 6B, where the coldest fiber in the wider radius geometry produces less condensate in all the cases considered, despite a larger temperature drop. This is due to the fact that geometries with wider radius have larger cross-sectional areas, and therefore a higher number of fibers. This lowers the gas flow through each fiber, reducing condensation.

The convection coefficient, h, clearly outweighs k_{trans} and Q, as the condensation rate is reduced by 90% within the considered range (Fig. 7). It is noticeable the fact that it would not be exaggerated to expect higher values than 10 W/m^2 K around the oxygenator in an operating theatre, due to the room ventilation required for anesthetic waste gas scavenging or microbiological control.

Regarding the combinations of best- and worst-case scenarios, the values of k_{trans}, h, and Q leading to a maximum ΔT are not the same that cause maximum condensation (Table 3). Interestingly, each one of the three parameters initially identified shows a different trend: k criterion changes in the worst case, but it remains equal in the best case; h

criterion remains the same for both the worst and the best cases; and Q criterion changes in both. It is particularly significant that the condensation rate and the maximum ΔT for the two worst cases differ by a factor around 2. For all the interactions described, it becomes clear that condensation process inside a blood oxygenator is hardly an intuitive phenomenon and that it should be considered in detail.

Some assumptions were taken regarding the boundary conditions of the computational model. In particular, the typical assumption of a uniform convection coefficient around the entire device was used, and no radiation was considered. Moreover, single values were considered for blood and room air temperature (37 and 20°C, respectively). Anyway, considering different thermal boundary conditions is not expected to modify the relative effect of the different parameters on water condensation.

Regarding the use of the Porous Media model, a more sophisticated approach would be needed which uses a composite thermal conductivity (15). However, the description of thermal conductivity in heterogeneous materials is out of the scope of this work. Indeed, considering the uncertainty in the properties of both the resin and the fiber membrane, together with the inherent limitations of the porous media, no further accuracy would be guaranteed. Moreover, it is significant that our analysis is valid for any microstructure of the fiber bundle, being the porosity ø not determinant in the simulations.

Finally, some attention should be paid to the assumption of constant gas flow through the fibers. The calculations in this study assume that the condensate is swept by the gas flow out of the fibers, and therefore fiber occlusion does not happen. Accounting for water presence in the fibers would require considering superficial tension effects inside the fiber lumen, together with the interactions of the membrane pores with the rainout drops, besides transient numerical simulations to represent the gas flow variations over time within each fiber. This treatment is clearly beyond the scope of this work, which aims to provide a first estimation of the condensation rate and to investigate the relative sensitivity of different parameters toward the overall effect.

Despite the above limitations, this model serves as a useful guideline for the design and clinical usage of the device, as it sheds light on the origin of the condensation effect, as well as quantifies the associated rates in different scenarios. Future work should be devoted to an experimental validation of the results to confirm the observed behaviors.

Acknowledgment: Ricardo Gómez Bardón is supported by the European Commission through the H2020 Marie Skłodowska-Curie European Training Network H2020-MSCA-ITN-2014 VPH-CaSE, www.vph-case.eu, GA No. 642612.

Conflict of Interest: The authors have no professional or financial conflicts of interest to disclose.

REFERENCES

1. Punjabi PP, Taylor KM. The science and practice of cardiopulmonary bypass: from cross circulation to ECMO and SIRS. *Glob Cardiol Sci Pract* 2013;2013:32.
2. Fang Y, Novak P, Hozalski R, Cussler E, Semmens M. Condensation studies in gas permeable membranes. *J Membr Sci* 2004;231:47–55.
3. Lund LW, Hattler BG, Federspiel WJ. Is condensation the cause of plasma leakage in microporous hollow fibre membrane oxygenators. *J Membr Sci* 1998;147:87–93.
4. Yamamura A, Watanabe M, Yoshida Y, Murakami M, Hurukawa H, Nakahara H. One formulation for a method of preventing a reduction in oxygenizing capability due to oxygenator condensation in long-term use of a PCPS. *Jpn J Extra Corpor Technol* 2005;32:50–2.
5. Anno M, Toda K, Maeda K, Nakajima T, Hanada T. About dewfall measures of PCPS. *Jpne J Extra Corpor Technol* 2010;37:436–9.
6. Nishigaki T, Fujii J, Yoshida K, et al. Prevention of dew condensation occurring in the oxygenator for extracorporeal life support in vitro model. *World Automation Congress (WAC)*. Puerto Vallarta, Mexico: IEEE, 2012. Available at: http://ieeexplore.ieee.org/articleDetails.jsp?arnumber=6320892
7. Kurashima N, Takeda H. Prototyping an automatic oxygen flush unit while using a PCPS. *Jpn J Extra Corpor Technol* 2000;27:13–5.
8. ANSYS Inc., 2016. Fluent User's Guide version 17.2. Canonsburg, PA.
9. Thomson G. The antoine equation for vapor-pressure data. *Chem Rev* 1946; 38:1–39.
10. Wickramasinghe SR, Han B, Garcia JD, Specht R. Microporous membrane blood oxygenators. *AIChE J* 2005;51:656–70.
11. Martínez L. Characterisation of three hydrophobic porous membranes used in membrane distillation Modelling and evaluation of their water vapour permeabilities. *J Membr Sci* 2002;203:15–27.
12. Qiu L, Zheng X, Yue P, et al. Adaptable thermal conductivity characterization of microporous membranes based on freestanding sensor-based 3-omega technique. *Int J Therm Sci* 2015;89:185–92.
13. Borges JC, Neto ML, Marinho GS. Variation of the thermal properties of a polyurethane-polyethylene composite. *J Phys Sci Appl* 2015;5:179–82.
14. Incropera FP, Incropera FP. *Fundamentals of Heat and Mass Transfer*. Hoboken, NJ: Wiley, 2007.
15. Wang J, Carson JK, North MF, Cleland DJ. A new approach to modelling the effective thermal conductivity of heterogeneous materials. *Int J Heat Mass Transf* 2006;49:3075–83.